Effects of Lipid Composition and Phase on the Membrane Interaction of the Prion Peptide 106–126 Amide

Jian Zhong,* Chunhui Yang, Wenfu Zheng, Lixin Huang, Yuankai Hong, Lijun Wang, and Yinlin Sha*
Single-Molecule and Nanobiology Laboratory, Department of Biophysics, School of Basic Medical Sciences, Biomed-X Center, and Center for Protein Science, Peking University, Beijing 100083, China

ABSTRACT Lipid rafts are specialized liquid-ordered (L_o) phases of the cell membrane that are enriched in sphingolipids and cholesterol (Chl), and surrounded by a liquid-disordered (L_d) phase enriched in glycerophospholipids. Lipid rafts are involved in the generation of pathological forms of proteins that are associated with neurodegenerative diseases. To investigate the effects of lipid composition and phase on the generation of pathological forms of proteins, we constructed an L_d-gel phase-separated 1-palmitoyl-2-oleoyl-*sn*-glycero-3-phosphocholine (POPC)/sphingomyelin (from bovine brain (BSM))-supported lipid bilayer (SLB) and an L_d-L_o phase-separated POPC/BSM/Chl SLB. We used in situ time-lapse atomic force microscopy to study the interactions between these SLBs and the prion peptide K^{106}TNMKHMAGAAAAGAVVGGLG^{126} (PrP106–126) amide, numbered according to the human prion-peptide sequence. Our results show that: 1), with the presence of BSM in the L_d phase, the PrP106–126 amide induces fully penetrated porations in the L_d phase of POPC/BSM SLB and POPC/BSM/Chl SLB; 2), with the presence of both BSM and Chl in the L_d phase, the PrP106–126 amide induces the disintegration of the L_d phase of POPC/BSM/Chl SLB; and 3), with the presence of both BSM and Chl in the L_o phase, PrP106–126 amide induces membrane thinning in the L_o phase of POPC/BSM/Chl SLB. These results provide comprehensive insight into the process by which the PrP106–126 amide interacts with lipid membranes.

INTRODUCTION

The ''fluid mosaic model'' for membrane structure was described in 1972 (1). It promoted an enormous development in the understanding of the structure and function of the cell membrane. Twenty-five years later, ''functional rafts'' (also named ''lipid rafts'') were proposed to exist as a specific liquid-ordered (L_o) phase enriched in sphingolipids and cholesterol (2). Since then, mounting scientific evidence has confirmed the presence of ''lipid rafts'' (3–6). Lipid rafts are clearly involved in the pathological processes of neurodegenerative diseases, including prion diseases (7–10) and Alzheimer's disease (10–12), but the specific pathological roles of these lipid rafts remain unclear.

Prion diseases are characterized by an accumulation of the abnormally misfolded, protease-resistant, β-sheet-rich pathological (scrapie) isoform (PrP^{Sc}) of the cellular prion protein (PrP^{c}) (13,14). Because full-length PrP^{Sc} is difficult to isolate and characterize, investigators often use synthetic K^{106}TNMKHMAGAAAAGAVVGGLG^{126} (PrP106–126) or an equivalent sequence as a substitute for PrP^{Sc} to study the physicochemical and pathological properties of PrP (15). Amino acids 106–126 are located in the unstructured N-terminal region, adjacent to the well-ordered globular domain of PrP. PrP106–126 appears to represent the neurotoxic core of PrP. The amphipathic primary structure of PrP106–126 is characterized by two distinct regions: an N-terminal hydrophilic region (K^{106}TNMKHM^{112}), and a C-terminal hydrophobic region (A^{113}GAAAAGAVVG GLG^{126}), providing favorable conditions for interacting with cell membranes (16). Alternately, PrP106–126 has many physiochemical qualities similar to those of PrP, including partial protease resistance, high β-sheet content, a propensity to form fibrils, and the ability to induce nerve-cell degeneration in a number of different primary-cell cultures (16–19). Reportedly, C-terminal amidation could significantly reduce the neurotoxicity of PrP106–126 (20–22). Considering the poor temporal resolution (in minutes) of atomic-force microscopy (AFM), the slow fibrogenesis kinetics of PrP106–126 amide (the C-terminal amidated form of PrP106–126) in physiological conditions (22) make it an ideal model for studying its properties in lipid membranes using in situ time-lapse AFM. Moreover, comprehensive insights into the neurotoxicity of PrP106–126 amide should arise.

Recent work indicated that PrP106–126 induces membrane neurotoxicity by inducing the formation of ion-specific permeable channels (23–25), membrane permeability, and destabilization (26). We previously demonstrated that interactions between PrP106–126 amide and a 1-palmitoyl-2-oleoyl-*sn*-glycero-3-phosphocholine (POPC) or POPC/cholesterol (Chl) membrane involve semipenetrated poration (27). Little attention has been paid to the effects of lipid rafts on peptide behavior (23–27). Clearly, additional studies are needed to understand the effects of changes in lipid structure and phase on membrane pore formation (27).

In situ time-lapse AFM is a powerful tool for studying the properties of membranes (28–33), the aggregation of

Submitted August 31, 2008, and accepted for publication January 23, 2009.

*Correspondence: shyl@hsc.pku.edu.cn or jianzhongpku@gmail.com

Jian Zhong is now a postdoctoral researcher at University College Dublin, Dublin, Ireland.

Editor: Petra Schwille.

0006-3495/09/06/4610/12 $2.00

doi: 10.1016/j.bpj.2009.01.036

amyloid peptides (34,35), interactions between proteins and membranes (36,37), and interactions between amyloid peptides and membranes (27,38–41). In particular, AFM can detect the phase separation of supported lipid bilayers (SLBs) (42,43). Therefore, it offers an excellent method for investigating lipid phases and biomolecular interactions with SLBs at the molecular scale. Triton X-100 is one of the most widely used nonionic detergents for purifying and classifying lipid rafts (44). Triton X-100 extraction is useful for differentiating phase separation in SLBs by AFM (31,32,45,46). Under the same conditions, the Triton X-100 resistances of specific phases are: L_o phase>gel phase>liquid-disordered (L_d) phase (32).

Sphingomyelin (SM) is enriched in lipid rafts in the outer leaflet of hippocampal neurons (47,48). Moreover, SM has the same hydrophilic headgroup as POPC, but a dissimilar hydrophobic backbone structure (49). Therefore, SM is a good model lipid for neurodegenerative diseases, and is also useful for investigating the hydrophobic backbone of lipids. Cholesterol (Chl) is an important constituent of lipid rafts, and plays an indispensable role in regulating the properties of eukaryotic cell membranes (3–5,10,50). Therefore, SM and Chl are good model cell lipids when constructing phase-separated SLBs. A phase diagram of the ternary system of POPC/SM/Chl at room temperature was described by De Almeida et al. (51) and Pokorny et al. (52).

We used brain sphingomyelin (BSM) and Chl to construct a L_d gel phase-separated POPC/BSM SLB and a L_d-L_o phase-separated POPC/BSM/Chl SLB. We used Triton X-100 extraction to validate the presence of different phases in SLBs. We confirmed previous results indicating that, under the same conditions, Triton X-100 resistances are: L_o phase>gel phase>L_d phase. Subsequently, we studied the interactions of PrP106–126 amide with SLBs, using in situ time-lapse AFM. We observed that, in contrast to semipenetrated porations in POPC or POPC/Chl SLBs (27), fully penetrated porations form in the L_d phase of POPC/BSM SLB and POPC/BSM/Chl SLB because of the presence of BSM. In addition, because of the presence of both BSM and Chl, PrP106–126 amide induces L_d phase membrane disintegration and L_o phase membrane thinning in POPC/BSM/Chl SLB. These results provide comprehensive insights into the process by which PrP106–126 interacts with lipid membranes. The possible mechanisms underlying interactions between PrP106–126 amide and POPC/BSM or POPC/BSM/Chl lipid bilayers are discussed in light of our results.

MATERIALS AND METHODS

Two different buffers were used for sample preparation and AFM imaging: HEPES-buffered saline (HBS)-1 (50 mM HEPES, 100 mM NaCl, and 2 mM $CaCl_2$, pH 7.4) and HBS-2 (50 mM HEPES and 100 mM NaCl, pH 7.4). All solutions were prepared with ultrapure water (18 MΩ · cm^{-1}), and all solutions were filtered through 0.2-μm filters before use. Synthetic POPC, BSM, and Chl were purchased from Sigma-Aldrich (Saint Louis, MO). We purchased 1-aminonaphthalene-3,6,8-trisulfonic acid (ANTS) and N, N′-*p*-xylylenebis (pyridinium) bromide (DPX) from Molecular Probes (Eugene, OR). The PrP106–126 amide was synthesized manually by F-moc chemistry and purified by reversed-phase-high-performance liquid chromatography, as described previously (27). The peptide was dissolved in water at a concentration of 2 mM, and immediately frozen at −20°C. The peptide stock solution was thawed before use, and never frozen again. When the stock solution was thawed and then dried on the freshly cleaved mica, no aggregation was observed according to AFM in air (data not shown).

Preparation of SLBs in HBS-2

The SLBs in HBS-2 were prepared by the vesicle fusion method, as described previously (27,53). Briefly, lipids were dissolved in chloroform/methanol (2:1, v/v), dried in a rotary evaporator, and kept under high vacuum overnight. The HBS-1 buffer at a volume of 400 μL was added to the bottle to hydrate the lipid (1.0 mg/mL), and the solution was vortexed vigorously until it became constantly milky. The solution was then extruded through a 0.1-μm polycarbonate membrane (Avanti Polar Lipids, Alabaster, AL) at 65°C, to obtain large unilamellar vesicles (LUVs). Next, 80 μL of LUV suspension were added to freshly cleaved mica (8 mm^2) and incubated at 70°C for 2 h. Finally, the sample was slowly cooled and then carefully rinsed with HBS-2 three times. The SLBs were maintained in an HBS-2 environment. According to our measurements, the SLBs were stable in HBS-2 for several days at room temperature.

The packing density of the POPC-rich lipid domain was ~0.46 nm^2 per lipid molecule, and the packing density of the BSM-rich lipid domain was ~0.39 nm^2 per lipid molecule (54). The amount of lipid on the mica surface (8 mm^2) was ~0.50 nmol. Because 10 random 10 × 10 μm-sized imaging fields of each SLB showed no defects, we assumed that the prepared SLBs had no defects. Because the total imaging volume of buffer was 100 μL, the lipid concentration on the mica surface was ~5.0 μM. Given that cholesterol packs into the acyl chains of lipid bilayers as a molecular spacer, the lipid concentration of POPC/BSM/Chl SLB on the mica surface should be similar to that of POPC/BSM SLB.

In situ time-lapse AFM

In situ time-lapse AFM images were acquired in the solution-tapping mode with a Nanoscope IV Multimode AFM (Veeco Instruments, Santa Barbara, CA) with an EV-scanner at room temperature, as described previously (27). We used sharpened OTR8 cantilevers (Veeco Instruments) with a nominal spring constant of 0.15 N/m. The frequency of the cantilever oscillation was tuned to 7–10 kHz, and the drive amplitude was adjusted to obtain a root mean-square value between 1.0–2.0 V. The height images were recorded at a 512 × 512 pixel resolution, and the scan rate was 1.49 Hz. After the addition of peptide (at a final concentration of 25 μM), the sample was immediately scanned from top to bottom. All in situ time-lapse AFM experiments were repeated three times on three independent bilayers. For every independent bilayer, one representative area (10 × 10 μm) was used for AFM experiments. All images were analyzed after treatment with ''flatten'' and ''plane fit auto'', using Nanoscope III software (version 5.12r2, Veeco Instruments). The height difference was measured using the ''section'' function, and the percentages of domain area and pores were analyzed using the ''bearing'' function in Nanoscope III software.

Detergent extraction

Triton X-100 stock solutions were prepared by dissolving Triton X-100 (16 mM) in water. These solutions were stored at room temperature. Detergent-extraction experiments were performed with in situ time-lapse AFM. Briefly, either POPC/BSM or POPC/BSM/Chl SLB was scanned and imaged in liquid tapping mode. The tip was lifted, and Triton X-100 stock solution was added, to a final concentration of 0.8 mM. The tip was engaged, and the sample was immediately scanned from top to bottom.

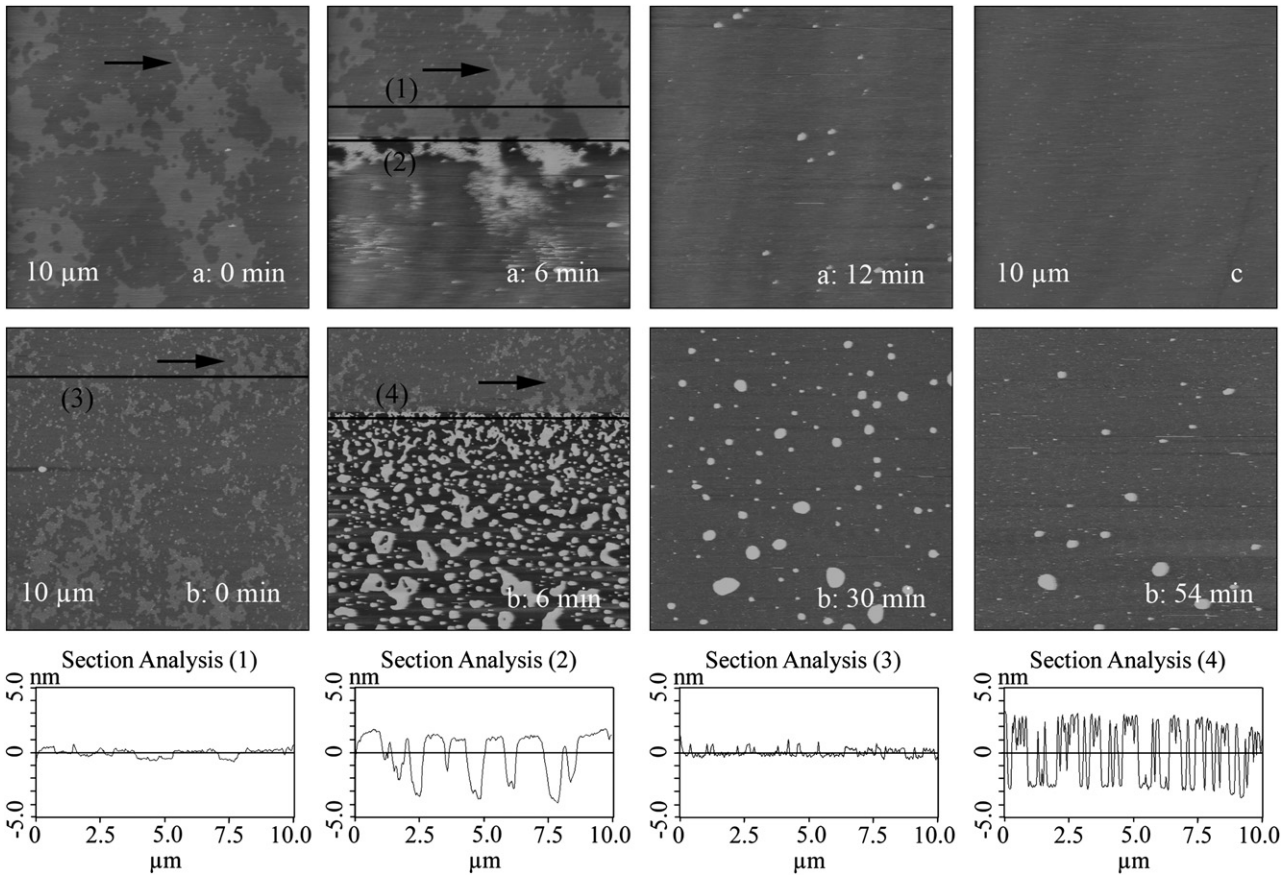

FIGURE 1 Construction and Triton X-100 extraction of SLBs. (*a*) In situ time-lapse AFM height images of Triton X-100 extraction of POPC/BSM (1:1, mol/mol) SLB. (*b*) In situ time-lapse AFM height images of Triton X-100 extraction of POPC/BSM/Chl (45:45:10, mol/mol/mol) SLB. (*c*) AFM height image of POPC/BSM/Chl (40:40:20, mol/mol/mol) SLB. Visual field is 10 × 10 μm. Height scale is 10 nm. Scan times before (0 min) and after injection of Triton X-100 are given in each image. Black arrows in *a* and *b* indicate same position before and after injection of Triton X-100. *Section Analysis (1)*: Gel phases are ~0.8 nm higher than L_d phases along black line in image of 6 min in *a*. *Section Analysis (2)*: gel phases are ~4.8 nm higher than the mica along the black line in image of 6 min in *a*. *Section Analysis (3)*: L_o phases are ~0.6 nm higher than L_d phases along black line in image of 0 min in *b*. *Section Analysis (4)*: L_o phases are ~5.4 nm higher than the mica along the black line in image of 6 min in *b*.

Permeability assay of LUVs

The permeability of lipid vesicles was measured using the ANTS/DPX assay, as described previously (27). Briefly, LUVs in a mixed solution (12.5 mM ANTS, 45 mM DPX, 50 mM HEPES, and 20 mM NaCl, pH 7.4) were prepared by extrusion through a 0.1-μm polycarbonate membrane with an extruder (Avanti Polar Lipids) at 65°C. Then the LUVs were separated from the unencapsulated ANTS and DPX with a HiTrap desalting column, using HBS-2 as elution buffer (Pharmacia Biotech AB, Uppsala, Sweden). The collected LUVs were diluted to a concentration below 100 μM. Fluorescence intensities were recorded with an F-4500 fluorescence spectrometer (Hitachi, Tokyo, Japan) after 20 min of PrP106–126 amide treatment. The excitation wavelength was set at 355 nm, and the emission wavelength was 512 nm. Fluorescence intensities corresponding to 0% and 100% leakage were determined before and after adding Triton X-100 (2.5%, v/v), respectively. All experiments were performed at 25°C.

Circular dichroism spectra

Circular dichroism (CD) spectra were recorded on a spectropolarimeter (model J-810, Jasco, Tokyo, Japan) at a peptide concentration of 50 μM under a 0.02-cm path length. Three scans were accumulated and automatically averaged in a wavelength range of 190–250 nm, with a 1-nm step resolution. For CD spectra of peptide in a lipid environment, the peptide/lipid molar ratio was 1:10. All CD spectra were measured at room temperature (25°C).

RESULTS AND DISCUSSION

Construction and Triton X-100 extraction of phase-separated model systems

A typical AFM height image of the POPC/BSM (1:1, mol/mol) SLB, whose composition is known via its phase diagram to produce L_d-gel phase separation at room temperature (51,52), is shown in Fig. 1 . Two coexisting phases are evident: the brighter domains correspond to the BSM-enriched gel phase, and the surrounding darker areas correspond to the POPC-enriched L_d phase. The gel phase comprised ~30.9% ± 6.8% of the bilayer (data were analyzed from 20 different 10 × 10 μm imaging fields of 12 independent bilayers). These data demonstrate that a proportion of BSM molecules was dispersed during the L_d phase (54). The height difference between the two phases was estimated at 0.8 ± 0.1 nm (n = 20; Fig. 1, *Section*

Analysis (1)), which agrees with previous data acquired in this lipid system using liquid AFM (29,55).

Here, we chose Triton X-100 extraction as a tool for validating the structures and properties of model membranes. A Triton X-100 solution was injected into the imaging solution, and then the SLB was immediately scanned (with scan direction from top to bottom). About 3 min after injection, the gel phase appeared to be considerably higher (Fig. 1 *a, 6 min*). It then gradually solubilized and disappeared. After 12 min, there were only a few spots (Fig. 1 *a*, *lighter spots*, *12 min*), demonstrating that the entire SLB was solubilized. The height of the gel phase above the mica was measured at ~4.8 nm (Fig. 1, *Section Analysis (2)*). Given that the height difference between the two phases was estimated at 0.8 ± 0.1 nm ($n = 20$; Fig. 1, *Section Analysis (1)*), the measured height of the L_d phase above the mica was found to be 4.0 nm, i.e., lower than that of a pure POPC L_d phase (~5.0 nm; data not shown).

The POPC/BSM/Chl (45:45:10, mol/mol/mol) SLB (Fig. 1 *b, 0 min*) was also observed to exist in two phases: brighter domains correspond to the BSM/Chl-enriched L_o phase, whereas the surrounding darker areas correspond to the POPC-enriched L_d phase. The gel domains, which should be present in the SLB according to the phase diagram of the ternary system of POPC/BSM/Chl (51,52), might not have been visible because their contribution was probably too small (56). The sizes of L_o phases were found to be small (several hundred nanometers in ''diameter''). These AFM results are similar to those obtained for the POPC/BSM/Chl (43:43:14, mol/mol/mol) SLB by Nicolini et al. (56). The L_o phase comprised ~20.5% ± 4.4% of the bilayer (data were analyzed from 20 different 10 × 10 μm imaging fields of 12 independent bilayers). These data demonstrated that a proportion of BSM molecules dispersed in the L_d phase (54). The measured height difference between the two phases was estimated at 0.6 ± 0.1 nm ($n = 20$; Fig. 1, *Section Analysis (3)*), i.e., a little lower than that between the gel and L_d phases in the POPC/BSM SLB. We also attempted to increase the proportion of Chl, but found that AFM could not detect the coexistence of two phases in a POPC/BSM/Chl (40:40:20, mol/mol/mol) SLB (Fig. 1 *c*).

We thought it best to use a phase-separation SLB to investigate interactions between peptides and the lipid membrane. Accordingly, we chose the POPC/BSM/Chl (45:45:10, mol/mol/mol) SLB for our in situ time-lapse AFM experiments. We also performed Triton X-100 extraction of the POPC/BSM/Chl (45:45:10, mol/mol/mol) SLB. In Fig. 1 *b*, (*6 min*), brighter domains (the L_o phase) appear to be considerably higher after ~2 min. Then the L_o phase is gradually solubilized and disappears (Fig. 1 *b*, *30 min* and *54 min*). The measured height difference between the L_o phase and the mica was 5.4 ± 0.1 nm ($n = 20$; see also Fig. 1 *Section Analysis (4)*). Given that the measured height difference between the two phases was estimated to be 0.6 ± 0.1 nm (n = 20, see also Fig. 1, *Section Analysis (3)*), the measured height of the L_d phase was ~4.8 nm.

Morandat and El Kirat (31) demonstrated that the gel phase of an L-α-dioleoylphosphatidylcholine (DOPC)/L-α-dipalmitoylphosphatidylcholine (DPPC) SLB does not completely disappear, even 70 min after adding 0.96 mM Triton X-100. El Kirat and Morandat (32) demonstrated that the gel phase of a DOPC/egg sphingomyelin (ESM) SLB does not completely disappear, even 120 min after the addition of Triton X-100, and the L_o phase of a DOPC/ESM/Chl SLB does not disappear, even 120 min after the addition of 0.96 mM Triton X-100. Here, however, the gel phase of the POPC/BSM SLB and the L_o phase of the POPC/BSM/Chl SLB disappeared a short time after adding 0.8 mM Triton X-100. This difference might be attributable to the different lipid sources. In both our study and theirs, the same Triton-100 resistances were observed, i.e., L_o phase>gel phase>L_d phase. Triton X-100 resistance depends on the stability of the lipid-lipid interaction relative to the lipid-Triton X-100 interaction (57). The molecular packing of BSM in the gel phase inhibits Triton X-100 insertion and Triton X-100/lipid micelle formation (31). Two independent factors concurrently inhibit the Triton X-100/lipid interaction in the L_o phase (58): 1), the molecular packing of BSM and Chl in the L_o phase (59–61); and 2), the molecular interactions between BSM and Chl, which are presumably hydrogen bonds between the carbonyl group of BSM and 3β-OH of Chl (62,63). Thus, interactions between BSM and Chl inhibit the insertion of Triton X-100 and the formation of Triton X-100/lipid micelles (32). These interactions increase the Triton X-100 resistance of the membrane. However, molecular packing forces and molecular interactions do not apply to POPC molecules in the L_d phase. Consequently, the L_o phase has the strongest resistance to Triton X-100. The gel phase is intermediate in resistance, and the L_d phase is least able to resist Triton X-100 perturbation.

Our results also show that Chl increases the measured height of membranes (Table 1). The measured height (4.8 nm) of the L_d phase of the POPC/SM/Chl SLB was found to be higher than that (4.0 nm) of the L_d phase of the POPC/SM SLB. The measured height (5.4 nm) of the L_o phase of the POPC/SM/Chl SLB was higher than that (4.8 nm) of the gel phase of the POPC/SM SLB. Moreover, the measured height difference (0.6 nm) between the different phases of the POPC/SM/Chl SLB was lower than that (0.8 nm) between the different phases of the POPC/SM SLB. This result is consistent with previous work (64). Cholesterol increases the length of POPC molecules by orientating them in a more perpendicular fashion (28,65). The BSM molecules cooperatively tilt in tandem during the gel phase. In the L_o phase, however, Chl intercalates between the chains of BSM, and thus reduces Chl's ability to tilt and thicken the BSM-enriched phases (65,66).

It is very important to be able to construct different lipid phase systems when studying a protein's interaction with the membrane. We constructed four different supported lipid bilayer model systems: POPC SLB and POPC/Chl SLB, as

TABLE 1 Measured heights of different phases

SLB	Measured height of L_d phase to mica (nm)	Measured height of BSM-enriched (gel or L_o) phase to mica (nm)	Height difference between different phases (nm)
POPC/BSM (45:45, mol/mol) SLB	4.0	4.8	0.8
POPC/BSM/Chl (45:45:10, mol/mol/mol) SLB	4.8	5.4	0.6

BSM-enriched phase is gel phase in POPC/BSM (45:45, mol/mol) SLB, and L_o phase in POPC/BSM/Chl (45:45:10, mol/mol/mol) SLB.

described previously (27), and POPC/BSM SLB and POPC/BSM/Chl SLB, as described here. We believe it is useful to investigate the effects that lipid composition and phase exert on the interactions between proteins/peptides and membranes. We can compare different phenomena in the same phase of different model membrane systems, or in different phases of the same model membrane system. Here, we constructed a series of SLB model systems to investigate interactions between proteins/peptides and membranes.

Fully penetrated poration in the L_d phase of a POPC/BSM SLB

To determine how BSM molecules affect interactions between the membrane and the PrP106–126 amide at the molecular level, we investigated interactions between PrP106–126 amide and the POPC/BSM (1:1, mol/mol) SLB with in situ time-lapse AFM (Fig. 2). After injecting PrP106–126 amide, pores appeared in the L_d phase at 60 min (Fig. 2, *b–d*). These pores were not visible at earlier times, even at 54 min (Fig. 2 *a*). Then, flat high-rise domains (FHDs), which we determined previously to be peptide/lipid phases induced by poration-medicated peptide diffusion in the hydrophobic region of the membrane (27), formed and diffused around the pores (Fig. 2, *white arrows*, *66 min*). Subsequently, FHDs expanded in size laterally, and gradually fused together over time (Fig. 2, *72*, *78*, *84*, and *108 min*). The FHDs comprised ~72.1%, and the gel phase comprised ~18.9%, of the bilayer in the 108-min image. The gel phase comprised ~26.9% of the bilayer in the 0-min image. Therefore, peptides can diffuse into the hydrophobic region of the gel phase and induce the formation and expansion of FHDs. At 108 min, we added Triton X-100 to the imaging solution, and immediately performed imaging. As in the L_d phase, FHDs were easily solubilized by Triton X-100 (Fig. 2, *Triton X-100*, *6 min*), indicating that the interactions between lipids and peptides were not sufficient to resist Triton X-100 extraction. The measured height of the gel phase from the mica was ~4.8 nm (Fig. 2, *Section Analysis (2)*), which is consistent with the measured height of the gel phase obtained earlier (Fig. 1 *a*, *Section Analysis (2)*). The measured height difference between the FHDs and the L_d phase was ~2.2 $\pm$ 0.1 nm ($n = 20$). The greatest depth of pores in the FHDs was ~5.6 nm (Fig. 2, *Section Analysis (1)*). The depth of pores relative to the top surface of the L_d phase was only 3.4 $\pm$ 0.1 nm. Because the measured height of the L_d phase was ~4.0 nm (analyzed according to Fig. 1 *a*), we assume that pores penetrated through the entire bilayer.

We also performed a leakage experiment with ANTS-DPX to investigate the effects of PrP106–126 amide on POPC/BSM membrane permeability (Fig. 3). Typically, for POPC/BSM LUVs, we observed 64% leakage at a peptide concentration of 50 μM, and 81% leakage at a peptide concentration of 100 μM. The results of this membrane permeability experiment are therefore consistent with the AFM data. Nonetheless, the ANTS-DPX leakage experiments and the in situ time-lapse AFM experiments showed that PrP106–126 amide induces semipenetrated poration in POPC or POPC/Chl SLBs (27). Consequently, BSM induces the formation of fully penetrated poration, just as SM increases the membrane permeability of melitin in the ANTS-DPX leakage assay (67). These results show that the poration mainly lies in the L_d phase, and rarely in the gel phase, at the initial time (only a few pores formed in the gel phase, e.g., the pore indicated by a black arrow in Fig. 2, *78 min*). Therefore, BSM in the L_d phase induces the formation of fully penetrated poration. The lag time (~60 min; Fig. 2) of poration in the POPC/SM SLB is longer than that (~18 min) (27) of poration in the pure POPC SLB, indicating that BSM increases the lag time of poration. In short, BSM has two functions during the interaction between PrP106–126 amide and POPC/SM SLB: 1), BSM induces the formation of fully penetrated poration in the L_d phase; and 2), BSM increases the lag time of poration.

To investigate the effect of lipids on the secondary structures of PrP106–126 amide, CD spectra were measured (Fig. 4) with PrP106–126 amide incubated for 0 or 180 min in three different environments: HBS-2, HBS-2-buffered POPC LUV, and HBS-2-buffered POPC/BSM LUV. The peptide/lipid molar ratio was 1:10. All spectra similarly presented a strong negative band at ~198 nm, i.e., a typical random-coil conformation. The results with HBS-2 are consistent with previous work (22). These results demonstrated that POPC and BSM do not change the random-coil conformation of PrP106–126 amide. The diffusions of FHDs and pores in POPC/BSM SLB are summarized in Fig. 5. The diffusion behavior resembles a part of a typical S-shaped curve (Fig. 5 *a*). After an initial lag phase, the average expansion rate of FHDs increases rapidly before 90 min (exponential growth phase), and decreases after 90 min (growth deceleration phase) (Fig. 5 *b*), in accordance with typical S-shaped growth-curve behavior (68). During the exponential growth phase, the percentage of pores

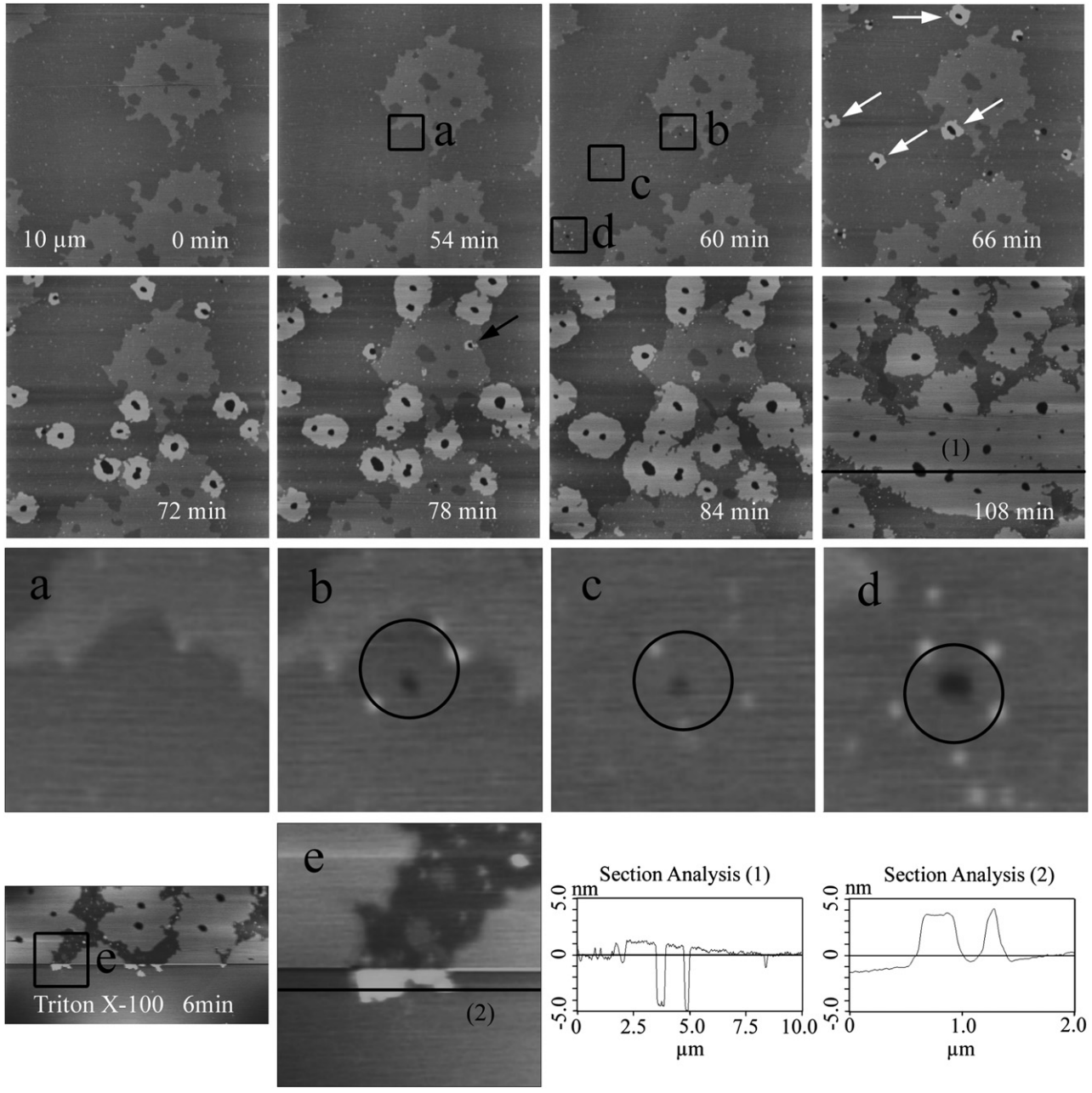

FIGURE 2 In situ time-lapse AFM images of PrP106–126 amide diffusion in POPC/BSM (1:1, mol/mol) SLB buffered by HBS-2. Visual field is 10 × 10 μm. Height scale is 10 nm. (*a–e*) Zoomed-in images from regions, with corresponding letter labels. Circles indicate formed pores. White arrows indicate FHDs. Black arrow indicates pore that occasionally forms during gel phase. *Section Analysis (1)*: depth of deepest pore in FHDs is ~5.6 nm along black line in image of 108 min. *Triton X-100, 6 min*: Triton X-100 extraction experiment after 108 min. *Section Analysis (2)*: gel phases are ~4.8 nm higher than the mica along the black line in image of Triton X-100 (*6 min*).

increases with time prolonging (Fig. 5 *c*). In addition, the average expansion rate of FHDs is proportionate to the average percentage of pores (Fig. 5 *d*), reflecting that pores sizes are more important in the diffusion of FHDs at lower peptide densities in the hydrophobic core of lipid bilayers (68). In the growth-deceleration phase, the slowing of the expansion rate (Fig. 5, *b* and *d*) reflects an increasing environmental (lipids and peptides) resistance that becomes proportionately more important at higher peptide densities in the hydrophobic core of lipid bilayers (68). The diffusion behavior of FHDs in POPC/BSM SLB is consistent with that of FHDs in POPC or POPC/Chl SLB (27).

We proposed a peptide-induced poration model for POPC and POPC/Chl membranes (27): the peptide binds to the POPC membrane surface, leading to an increase of strain on the membrane surface. Semipenetrated pores then form to reduce this strain. The change from semipenetrated poration in the POPC SLB to fully penetrated poration in the POPC/BSM

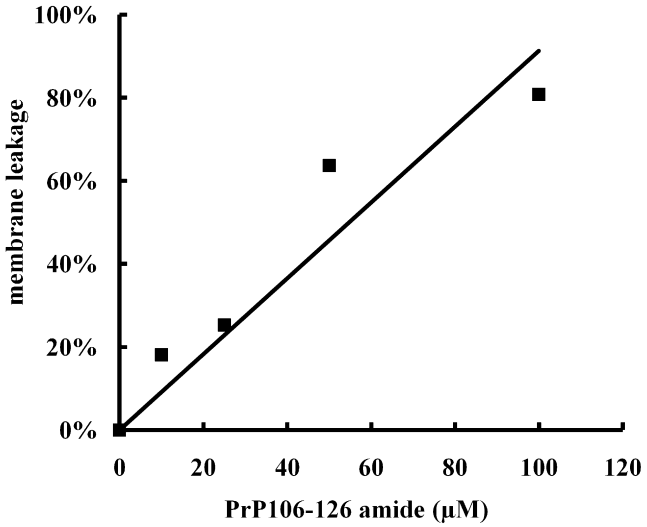

FIGURE 3 Leakage of vesicle contents (ANTS/DPX) of a POPC/BSM (1:1, mol:mol) LUV was induced by different concentrations of PrP106–126 amide at 25°C. Line on the graph is trendline of membrane leakage versus peptide concentration.

SLB implies that fully penetrated poration undergoes two semipenetrated porations: first, an upper leaflet-penetrated poration, and then, lower leaflet-penetrated poration. Our data regarding the POPC/BSM SLB show that porations mainly lie in the L_d phase, and rarely in the gel phase. Compared with a pure POPC SLB, a POPC/BSM SLB has a portion of BSM molecules that are dispersed in the L_d phase. In the L_d phase, BSM and POPC have the same membrane surface-peptide binding ability because they have identical hydrophilic heads. The binding of POPC to peptide easily leads to a lateral expansion of the bilayer and a thinning of the hydrophobic lipid core (69–71), which increases the membrane strain. The sphingosine backbone of SM is more rigid than the glycerol backbone of POPC, so the binding of a peptide to an SM surface is less likely to increase membrane strain. The presence of SM slows the formation of membrane strain in the L_d phase. As a consequence, the lag time of poration (~60 min; Fig. 2) is longer than that in a pure POPC SLB (~18 min) (27). When semipenetrated poration forms on the upper leaflet of a POPC or POPC/Chl SLB, the peptide can bind the exposed lipids on the lower leaflet to stabilize the pores immediately, completing the formation of semipenetrated poration (27). When upper leaflet-penetrated poration forms in the L_d phase of a POPC/BSM SLB, however, a peptide is less able to insert into the hydrophobic core because of the rigidity of sphingosine. Therefore, the peptide cannot bind the exposed backbones of BSM lipids on the lower leaflet to stabilize the pores, and the exposed BSMs and surrounding lipids are quickly released, causing a poration on the lower leaflet of SLB. Therefore, fully penetrated porations form during the L_d phase of a POPC/BSM SLB.

In the gel phase, because of the rigidity and tight packing of sphingosine, BSM surface-peptide binding ability may be

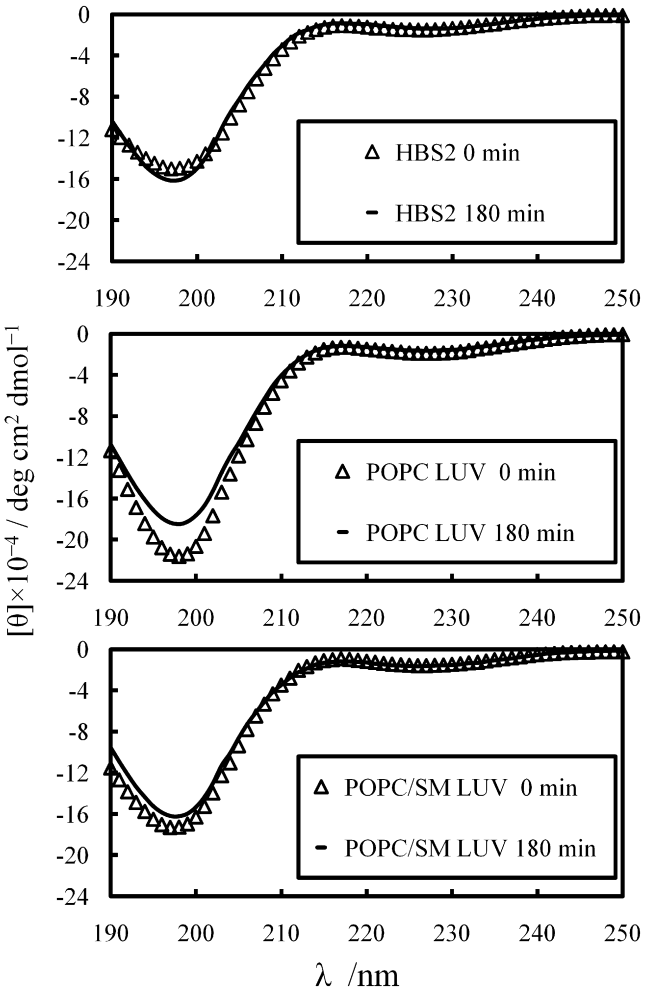

FIGURE 4 The CD spectra of PrP106–126 amide incubated for 0 min or 180 min in three different environments (HBS-2, HBS-2-buffered POPC LUV, and HBS-2-buffered POPC/SM LUV). All CD spectra present negative adsorption at ~198 nm, a typical characteristic of random coils. λ: wavelength.

lower than that of BSM in the L_d phase. Therefore, poration does not occur efficiently in the gel phase. A small portion of POPC molecules, however, do disperse in the gel phase (54). Binding to peptide in the gel phase could induce membrane strain. The formation of pores occurred occasionally in the gel phase at initial time periods (Fig. 2, *black arrow*, *78 min*). These results indicate that the formation of pores in the gel phase is less likely than in the L_d phase. After peptides diffuse into the L_d phase through pores, however, they can diffuse into the hydrophobic region of the gel phase and induce the formation and expansion of FHDs.

To summarize, our results suggest that interactions between PrP106–126 amide and a POPC/BSM SLB may involve fully penetrated poration-mediated FHD diffusion, which mainly occurs in the L_d phase because of the presence of BSM (see Fig. 7 *a*). First, the peptide binds to the headgroup region of lipids in the L_d phase of the membrane. The binding of peptide to the POPC surface increases membrane

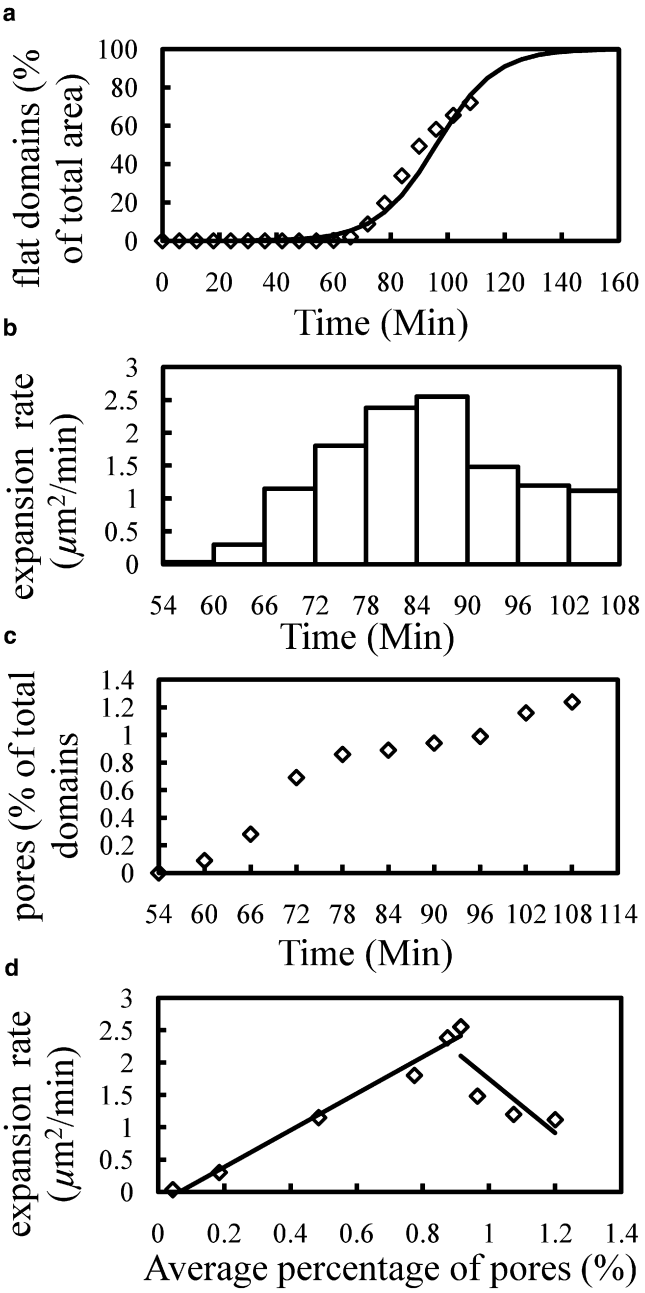

FIGURE 5 Diffusions of FHDs and pores. (*a*) Area percentage (◇) of FHDs as a function of time. The line on the graph is a typical S-shaped curve: $y = 100/[1 + 10{,}112 * \exp(-0.096 * x)]$, where y is percentage of FHD area at time x min. (*b*) Average expansion rate of FHDs during AFM imaging interval (every 6 min). (*c*) Percentage (◇) of pores as a function of time. (*d*) Average expansion rate of FHDs versus average percentage of pores during AFM imaging interval (every 6 min). Data were fitted by a linear equation ($y = a * x + b$). In the exponential growth phase, $y = 2.84x - 0.183$, $R^2 = 0.985$; in the growth deceleration phase, $y = -4.189x + 5.939$, $R^2 = 0.644$.

strain. The binding of peptide to the BSM surface does not, however, increase membrane strain. Second, when a threshold concentration of peptide on the surface of the L_d phase is reached, the membrane releases vesicles containing the peptide-upper leaflet lipid complex, causing upper leaflet-penetrated poration and reducing the strain imposed on the bilayer by the presence of the peptide chain. Third, near the upper leaflet-penetrated pore, peptide binds to the exposed POPC lipids, but not immediately to the exposed BSM lipid hydrophobic core. Because the pores cannot be stabilized in time, the lower leaflet continues to form lower leaflet-penetrated pores. Therefore, fully penetrated pores form during the L_d phase. At the same time, the peptide quickly diffuses through the pores into the hydrophobic region of the L_d phase of the lipid bilayer, and finally into the gel phase, as indicated by the formation and expansion of FHDs.

Fully penetrated poration in POPC/BSM/Chl SLB

We also investigated the interaction between PrP106–126 amide and a POPC/BSM/Chl (45:45:10, mol/mol/mol) SLB (Fig. 6). After the injection of PrP106–126 amide, the L_o phase disappeared. Pores and FHDs appeared (Fig. 6, *18 min*). Subsequently, the SLB was quickly ruined (Fig. 6, *24 min* and *30 min*). In fact, we were unable to engage the probe of AFM at the surface of the SLB until ~12 min, perhaps because of a block from the lipid-peptide vesicles that were quickly released. The measured height difference between FHDs and the top surface of the L_d phase was 2.2 ± 0.1 nm ($n = 20$), which is similar to what was observed in the POPC/BSM SLB-peptide interaction experiments. The deepest pores on the FHDs were ~6.4 nm (Fig. 6, *Section Analysis (1)*). Thus, the depth of pores from the top surface of the L_d phase was 4.2 nm. Considering that the measured height of the L_d phase of the POPC/BSM/Chl SLB was 4.8 nm (analyzed according to Fig. 1 *b*), it appears that pores penetrated the entire bilayer. This result is similar to that observed for the POPC/BSM SLB. The BSM in the L_d phase induced the formation of fully penetrated poration in the L_d phase of POPC/BSM SLB. It is reasonable to speculate that the BSM in the L_d phase induced the formation of fully penetrated poration in the L_d phase of the POPC/BSM/Chl SLB via a similar mechanism. Firstly, the interaction between peptide and POPC induces upper leaflet-penetrated porations. Then, BSM affects the interaction between peptide and membrane, to form lower leaflet-penetrated porations. In a POPC/BSM/Chl SLB, the pores are obviously bigger (on a micrometer scale; Fig. 6, *18 min* and *24 min*) than in a POPC/BSM SLB (Fig. 2). The sizes increase with time until the whole SLB is nearly ruined (Fig. 6, *30 min*). The POPC/Chl SLB-peptide interaction, which we investigated previously (27), and the POPC/BSM SLB-peptide interaction (Fig. 2), which we present here, do not cause disintegration of the membrane. We conclude that with the presence of both BSM and Chl, PrP106–126 amide induces membrane disintegration. The interaction between BSM and Chl, which are presumably hydrogen bonds between the carbonyl group of BSM and 3β-OH of Chl (62,63), might be the main cause of inducing membrane

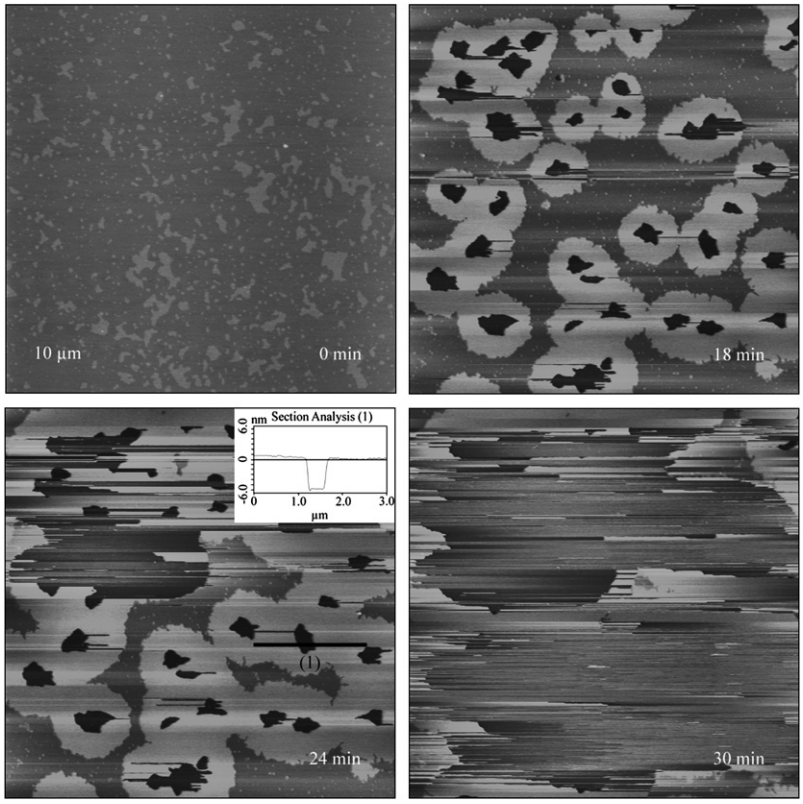

FIGURE 6 In situ time-lapse AFM height images of PrP106–126 amide diffusion on a POPC/BSM/Chl (45:45:10, mol/mol/mol) SLB buffered by HBS-2. Visual field is 10 × 10 μm. Height scale is 10 nm. Scan times before (0 min) and after the injection of peptide are given in each image. To show complete height of a pore, the height scale of Section Analysis (1) was adjusted to 13 nm. *Section Analysis (1)*: FHDs are ~6.4 nm higher than the mica along the black line in the image of 24 min.

disintegration. When fully penetrated pores and FHDs form in the L_d phase, the binding of peptide to BSM and Chl may be not stable, and membrane disintegration occurs.

At 0 min, many L_o domains were dispersed in the L_d phase. At 18 min, however, only pores, FHDs, and the L_d phase were present. No L_o phases were dispersed in the L_d phase, implying that the binding of peptide to the L_o phase surface led to membrane thinning (36,69–71). The height of the membrane-thinning domain is the same as the height of the L_d phase. Three mechanisms were proposed to explain peptide-induced membrane thinning (69): 1), the formation of a lower leaflet/peptide complex reduces the height of membrane-thinning domains to about half that of the original membrane; 2), the formation of an asymmetric lipid bilayer by lipid flip-flop reduces the height of membrane-thinning domains to a height between that of the L_o phase and of the L_d phase; and 3), an interdigitation of bilayers occurs. We observed the same height between the membrane-thinning domain and the L_d phase, ruling out mechanisms 1 and 2. The only possible mechanism is the interdigitation of bilayers, which induces the height of membrane-thinning domains to be equal to that of the L_d phase of the POPC/BSM/Chl SLB. The POPC/Chl SLB-peptide interaction, as investigated previously (27), and the POPC/BSM SLB-peptide interaction (Fig. 2), which we present here, do not cause membrane thinning. We conclude, therefore, that with the presence of both BSM and Chl in the L_o phase, PrP106–126 amide induces membrane thinning. Two reasons may be responsible for the membrane thinning: 1), PrP106–126 amide can induce membrane thinning during the L_o phase; and 2), the interaction between BSM and Chl, which are presumably hydrogen bonds between the carbonyl group of BSM and 3β-OH of cholesterol (62,63), may induce membrane thinning. When peptide interacts with BSM and Chl in the L_o phase, it can insert into the hydrophobic core of the L_o phase and induce membrane thinning.

In addition to the differences already noted between the POPC/BSM/Chl SLB and POPC/BSM SLB, there are three others: 1), the lag time of poration (<18 min) in the POPC/BSM/Chl SLB was shorter than that (~60 min) in the POPC/BSM SLB; 2), in midphase, more pores were formed in the POPC/BSM/Chl SLB; and 3), the diffusion of FHDs in the POPC/BSM/Chl SLB was faster than in the POPC/BSM SLB. This comparison resembles that between the POPC/Chl SLB and the POPC SLB (27). These differences strengthen our previous hypothesis that Chl increases the quantity of poration and decreases the rate of poration by decreasing the threshold concentration of peptide for SLB poration (27). This lowering of the threshold decreases the lag time of poration in a Chl-containing SLB, compared with a SLB without Chl.

We propose that the interaction between PrP106–126 amide and a POPC/BSM/Chl SLB involves membrane thinning in the L_o phase, fully penetrated poration-mediated FHD diffusion, and membrane disintegration in the L_d phase (Fig. 7 *b*). First, the peptide binds to the lipid headgroups on

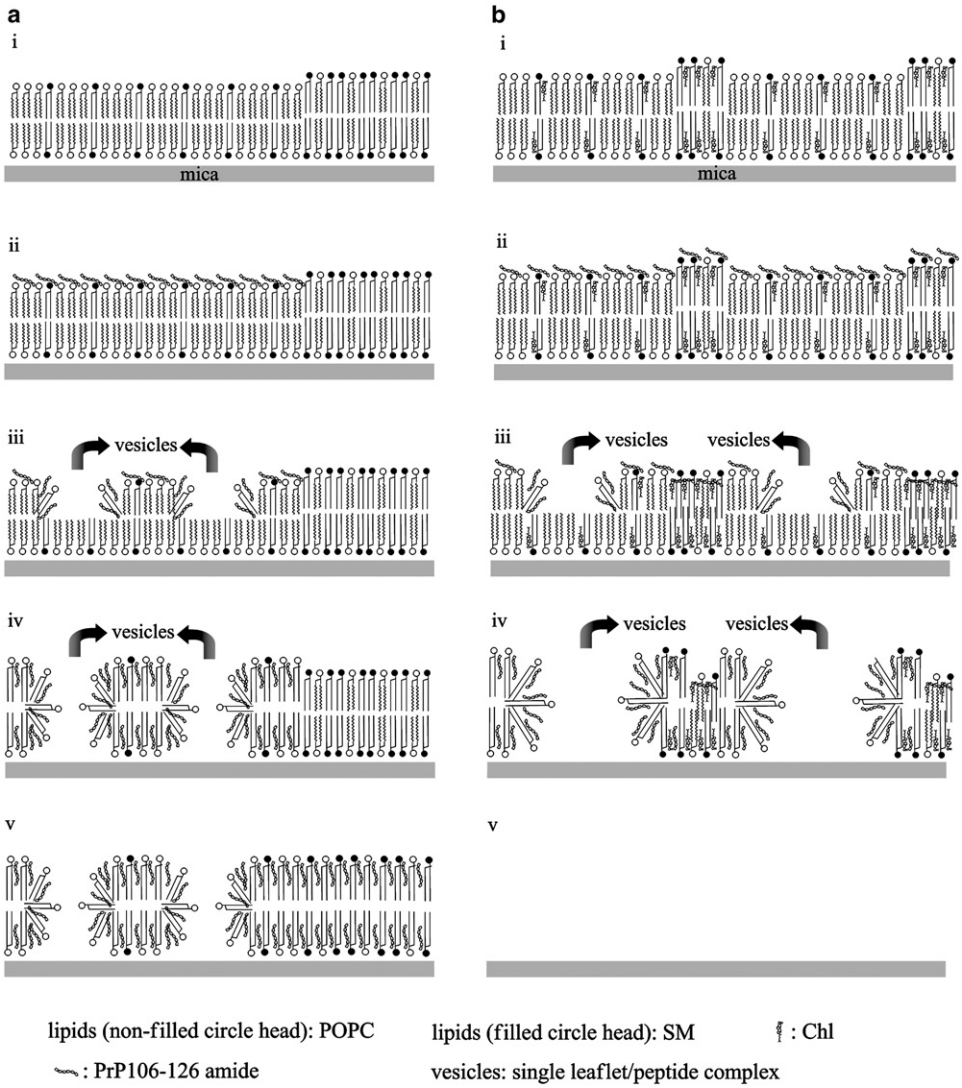

FIGURE 7 Schematics of possible mechanisms by which PrP106–126 amide interacts with SLBs. (*a*) Interaction between POPC/BSM SLB and peptide. (*b*) Interaction between POPC/BSM/Chl SLB and peptide. See text for details.

the membrane surface. Second, in the L_o phase, binding quickly leads to membrane thinning; the height of the L_o phase membrane-thinning domain equals that of the L_d phase. To reduce the membrane strain induced by the peptide binding to the membrane surface, the L_d phases release vesicles of the peptide and upper-leaflet lipid. Third, because of the presence of BSM, the vesicles of the peptide and lower-leaflet lipid are released to cause fully penetrated poration. At the same time, the peptide quickly diffuses into the lipid bilayer through the pores, as indicated by the formation and expansion of FHDs. Fourth, because of the presence of BSM and Chl in the L_d phase, membrane disintegration occurs. The membrane-thinning domains are also ruined.

This study relied only on AFM and membrane-permeability experiments. Further work using fluorescence microscopy will be necessary to address the start position of poration and peptide diffusion in the membrane. Additional studies must address the destabilization of living cell membranes by peptide binding, and would increase our understanding of the membrane perturbation caused by PrP106–126 amide. Differing from the semipenetrated poration observed in POPC and POPC/Chl SLBs, fully penetrated poration is induced by PrP106–126 amide in a POPC/BSM SLB and a POPC/BSM/Chl SLB. Our studies offer powerful support for the hypothesis that lipid structure and membrane phases have enormous effects on the generation of pathological forms of proteins in neuronal diseases.

We thank Chuang Liu, Xiaoli Liu, Ruibin Zhang, Ruirui Qiao, Lan Zhang, Rongcheng Han, Ying Liu, and Min Yu for helpful discussions.

This work was supported by grants from the Natural Science Foundation of China (projects 20273002 and 20103001).

REFERENCES

1. Singer, S. J., and G. L. Nicolson. 1972. The fluid mosaic model of the structure of cell membranes. *Science*. 175:720–731.
2. Simons, K., and E. Ikonen. 1997. Functional rafts in cell membranes. *Nature*. 387:569–572.

3. Simons, K., and D. Toomre. 2000. Lipid rafts and signal transduction. *Nat. Rev. Mol. Cell Biol.* 1:31–39.
4. Edidin, M. 2003. Lipids on the frontier: a century of cell-membrane bilayers. *Nat. Rev. Mol. Cell Biol.* 4:414–418.
5. Jacobson, K., O. G. Mouritsen, and R. G. Anderson. 2007. Lipid rafts: at a crossroad between cell biology and physics. *Nat. Cell Biol.* 9:7–14.
6. van Meer, G., D. R. Voelker, and G. W. Feigenson. 2008. Membrane lipids: where they are and how they behave. *Nat. Rev. Mol. Cell Biol.* 9:112–124.
7. Taylor, D. R., and N. M. Hooper. 2006. The prion protein and lipid rafts. *Mol. Membr. Biol.* 23:89–99.
8. Vey, M., S. Pilkuhn, H. Wille, R. Nixon, S. J. Dearmond, et al. 1996. Subcellular colocalization of the cellular and scrapie prion proteins in caveolae-like membranous domains. *Proc. Natl. Acad. Sci. USA.* 93:14945–14949.
9. Taraboulos, A., M. Scott, A. Semenov, D. Avraham, L. Laszlo, et al. 1995. Cholesterol depletion and modification of COOH-terminal targeting sequence of the prion protein inhibit formation of the scrapie isoform. *J. Cell Biol.* 129:121–132.
10. Fantini, J., N. Garmy, R. Mahfoud, and N. Yahi. 2002. Lipid rafts: structure, function and role in HIV, Alzheimer's and prion diseases. *Expert Rev. Mol. Med.* 2002:1–22.
11. Cordy, J. M., N. M. Hooper, and A. J. Turner. 2006. The involvement of lipid rafts in Alzheimer's disease. *Mol. Membr. Biol.* 23:111–122.
12. Marchesi, V. T. 2005. An alternative interpretation of the amyloid A beta hypothesis with regard to the pathogenesis of Alzheimer's disease. *Proc. Natl. Acad. Sci. USA.* 102:9093–9098.
13. Prusiner, S. B. 1998. Prions. *Proc. Natl. Acad. Sci. USA.* 95:13363–13383.
14. Dobson, C. M. 2003. Protein folding and misfolding. *Nature.* 426:884–890.
15. Brown, D. R. 2002. Mayhem of the multiple mechanisms: modelling neurodegeneration in prion disease. *J. Neurochem.* 82:209–215.
16. De Gioia, L., C. Selvaggini, E. Ghibaudi, L. Diomede, O. Bugiani, et al. 1994. Conformational polymorphism of the amyloidogenic and neurotoxic peptide homologous to residues 106–126 of the prion protein. *J. Biol. Chem.* 269:7859–7862.
17. Brown, D. R., B. Schmidt, and H. A. Kretzschmar. 1996. Role of microglia and host prion protein in neurotoxicity of a prion protein fragment. *Nature.* 380:345–347.
18. Forloni, G., N. Angeretti, R. Chiesa, E. Monzani, M. Salmona, et al. 1993. Neurotoxicity of a prion protein fragment. *Nature.* 362:543–546.
19. Brown, D. R., J. Herms, and H. A. Kretzschmar. 1994. Mouse cortical cells lacking cellular PrP survive in culture with a neurotoxic PrP fragment. *Neuroreport.* 5:2057–2060.
20. Heegaard, P. M. H., H. G. Pedersen, J. Flink, and U. Boas. 2004. Amyloid aggregates of the prion peptide PrP106–126 are destabilised by oxidation and by the action of dendrimers. *FEBS Lett.* 577:127–133.
21. Bergstrom, A. L., H. Cordes, N. Zsurger, P. M. H. Heegaard, H. Laursen, et al. 2005. Amidation and structure relaxation abolish the neurotoxicity of the prion peptide PrP106–126 in vivo and in vitro. *J. Biol. Chem.* 280:23114–23121.
22. Salmona, M., P. Malesani, L. De Gioia, S. Gorla, M. Bruschi, et al. 1999. Molecular determinants of the physicochemical properties of a critical prion protein region comprising residues 106–126. *Biochem. J.* 342:207–214.
23. Lin, M. X., T. Mirzabekov, and B. L. Kagan. 1997. Channel formation by a neurotoxic prion protein fragment. *J. Biol. Chem.* 272:44–47.
24. Kagan, B. L., R. Azimov, and R. Azimova. 2004. Amyloid peptide channels. *J. Membr. Biol.* 202:1–10.
25. Kourie, J. I., and A. A. Shorthouse. 2000. Properties of cytotoxic peptide-formed ion channels. *Am. J. Physiol. Cell Physiol.* 278:C1063–C1087.
26. Dupiereux, I., W. Zorzi, L. Lins, R. Brasseur, P. Colson, et al. 2005. Interaction of the 106–126 prion peptide with lipid membranes and potential implication for neurotoxicity. *Biochem. Biophys. Res. Commun.* 331:894–901.
27. Zhong, J., W. Zheng, L. Huang, Y. Hong, L. Wang, et al. 2007. PrP106–126 amide causes the semi-penetrated poration in the supported lipid bilayers. *Biochim. Biophys. Acta.* 1768:1420–1429.
28. Lawrence, J. C., D. E. Saslowsky, J. M. Edwardson, and R. M. Henderson. 2003. Real-time analysis of the effects of cholesterol on lipid raft behavior using atomic force microscopy. *Biophys. J.* 84:1827–1832.
29. Giocondi, M. C., P. E. Milhiet, P. Dosset, and C. Le Grimellec. 2004. Use of cyclodextrin for AFM monitoring of model raft formation. *Biophys. J.* 86:861–869.
30. Chiantia, S., N. Kahya, and P. Schwille. 2005. Dehydration damage of domain-exhibiting supported bilayers: an AFM study on the protective effects of disaccharides and other stabilizing substances. *Langmuir.* 21:6317–6323.
31. Morandat, S., and K. El Kirat. 2006. Membrane resistance to Triton X-100 explored by real-time atomic force microscopy. *Langmuir.* 22:5786–5791.
32. El Kirat, K., and S. Morandat. 2007. Cholesterol modulation of membrane resistance to Triton X-100 explored by atomic force microscopy. *Biochim. Biophys. Acta.* 1768:2300–2309.
33. Lin, W. C., C. D. Blanchette, T. V. Ratto, and M. L. Longo. 2006. Lipid asymmetry in DLPC/DSPC-supported lipid bilayers: a combined AFM and fluorescence microscopy study. *Biophys. J.* 90:228–237.
34. Kowalewski, T., and D. M. Holtzman. 1999. In situ atomic force microscopy study of Alzheimer's beta-amyloid peptide on different substrates: new insights into mechanism of beta-sheet formation. *Proc. Natl. Acad. Sci. USA.* 96:3688–3693.
35. Parbhu, A., H. Lin, J. Thimm, and R. Lal. 2002. Imaging real-time aggregation of amyloid beta protein (1–42) by atomic force microscopy. *Peptides.* 23:1265–1270.
36. You, H. X., X. Y. Qi, G. A. Grabowski, and L. Yu. 2003. Phospholipid membrane interactions of saposin C: in situ atomic force microscopic study. *Biophys. J.* 84:2043–2057.
37. Morandat, S., and K. El Kirat. 2007. Real-time atomic force microscopy reveals cytochrome *c*–induced alterations in neutral lipid bilayers. *Langmuir.* 23:10929–10932.
38. Yip, C. M., A. A. Darabie, and J. McLaurin. 2002. A beta 42-peptide assembly on lipid bilayers. *J. Mol. Biol.* 318:97–107.
39. Yip, C. M., E. A. Elton, A. A. Darabie, M. R. Morrison, and J. McLaurin. 2001. Cholesterol, a modulator of membrane-associated A beta-fibrillogenesis and neurotoxicity. *J. Mol. Biol.* 311:723–734.
40. Yip, C. M., and J. McLaurin. 2001. Amyloid-beta peptide assembly: a critical step in fibrillogenesis and membrane disruption. *Biophys. J.* 80:1359–1371.
41. Green, J. D., L. Kreplak, C. Goldsbury, X. L. Blatter, M. Stolz, et al. 2004. Atomic force microscopy reveals defects within mica supported lipid bilayers induced by the amyloidogenic human amylin peptide. *J. Mol. Biol.* 342:877–887.
42. Dufrene, Y. F., and G. U. Lee. 2000. Advances in the characterization of supported lipid films with the atomic force microscope. *Biochim. Biophys. Acta.* 1509:14–41.
43. Connell, S. D., and D. A. Smith. 2006. The atomic force microscope as a tool for studying phase separation in lipid membranes. *Mol. Membr. Biol.* 23:17–28 [Review].
44. Chamberlain, L. H. 2004. Detergents as tools for the purification and classification of lipid rafts. *FEBS Lett.* 559:1–5.
45. Rinia, H. A., and B. de Kruijff. 2001. Imaging domains in model membranes with atomic force microscopy. *FEBS Lett.* 504:194–199.
46. Garner, A. E., D. A. Smith, and N. M. Hooper. 2008. Visualization of detergent solubilization of membranes: implications for the isolation of rafts. *Biophys. J.* 94:1326–1340.
47. Wood, W. G., F. Schroeder, U. Igbavboa, N. A. Avdulov, and V. V. Chochina. 2002. Brain membrane cholesterol domains, aging and amyloid beta-peptides. *Neurobiol. Aging.* 23:685–694.

48. Palestini, P., L. Botto, F. Guzzi, C. Calvi, D. Ravasi, et al. 2002. Developmental changes in the protein composition of sphingolipid- and cholesterol-enriched membrane domains of rat cerebellar granule cells. *J. Neurosci. Res.* 67:729–738.

49. Lambert, T. N., and B. D. Smith. 2003. Synthetic receptors for phospholipid headgroups. *Coord. Chem. Rev.* 240:129–141.

50. Simons, K., and E. Ikonen. 2000. How cells handle cholesterol. *Science.* 290:1721–1726.

51. de Almeida, R. F. M., A. Fedorov, and M. Prieto. 2003. Sphingomyelin/phosphatidylcholine/cholesterol phase diagram: boundaries and composition of lipid rafts. *Biophys. J.* 85:2406–2416.

52. Pokorny, A., L. E. Yandek, A. I. Elegbede, A. Hinderliter, and P. F. F. Almeida. 2006. Temperature and composition dependence of the interaction of delta-lysin with ternary mixtures of sphingomyelin/cholesterol/POPC. *Biophys. J.* 91:2184–2197.

53. Zhang, L., J. Zhong, L. Huang, L. Wang, Y. Hong, et al. 2008. Parallel-oriented fibrogenesis of a β-sheet forming peptide on supported lipid bilayers. *J. Phys. Chem.* 112:8950–8954.

54. Salamon, Z., S. Devanathan, I. D. Alves, and G. Tollin. 2005. Plasmon-waveguide resonance studies of lateral segregation of lipids and proteins into microdomains (rafts) in solid-supported bilayers. *J. Biol. Chem.* 280:11175–11184.

55. Giocondi, M. C., S. Boichot, T. Plenat, and C. Le Grimellec. 2004. Structural diversity of sphingomyelin microdomains. *Ultramicroscopy.* 100:135–143.

56. Nicolini, C., J. Baranski, S. Schlummer, J. Palomo, M. Lumbierres-Burgues, et al. 2006. Visualizing association of N-Ras in lipid microdomains: influence of domain structure and interfacial adsorption. *J. Am. Chem. Soc.* 128:192–201.

57. London, E., and D. A. Brown. 2000. Insolubility of lipids in Triton X-100: physical origin and relationship to sphingolipid/cholesterol membrane domains (rafts). *Biochim. Biophys. Acta.* 1508:182–195.

58. Sot, J., M. I. Collado, J. L. R. Arrondo, A. Alonso, and F. M. Goni. 2002. Triton X-100-resistant bilayers: effect of lipid composition and relevance to the raft phenomenon. *Langmuir.* 18:2828–2835.

59. Crane, J. M., and L. K. Tamm. 2004. Role of cholesterol in the formation and nature of lipid rafts in planar and spherical model membranes. *Biophys. J.* 86:2965–2979.

60. Silvius, J. R. 2003. Role of cholesterol in lipid raft formation: lessons from lipid model systems. *Biochim. Biophys. Acta.* 1610:174–183.

61. Maxfield, F. R., and I. Tabas. 2005. Role of cholesterol and lipid organization in disease. *Nature.* 438:612–621.

62. Slotte, J. P. 1999. Sphingomyelin-cholesterol interactions in biological and model membranes. *Chem. Phys. Lipids.* 102:13–27.

63. Veiga, M. P., J. L. R. Arrondo, F. M. Goni, A. Alonso, and D. Marsh. 2001. Interaction of cholesterol with sphingomyelin in mixed membranes containing phosphatidylcholine, studied by spin-label ESR and IR spectroscopies. A possible stabilization of gel-phase sphingolipid domains by cholesterol. *Biochemistry.* 40:2614–2622.

64. Milhiet, P. E., M. C. Giocondi, and C. Le Grimellec. 2002. Cholesterol is not crucial for the existence of microdomains in kidney brush-border membrane models. *J. Biol. Chem.* 277:875–878.

65. Sprong, H., P. van der Sluijs, and G. van Meer. 2001. How proteins move lipids and lipids move proteins. *Nat. Rev. Mol. Cell Biol.* 2:504–513.

66. Samsonov, A. V., I. Mihalyov, and F. S. Cohen. 2001. Characterization of cholesterol-sphingomyelin domains and their dynamics in bilayer membranes. *Biophys. J.* 81:1486–1500.

67. Gomara, M. J., S. Nir, and J. L. Nieva. 2003. Effects of sphingomyelin on melittin pore formation. *Biochim. Biophys. Acta.* 1612:83–89.

68. Britton, N. F. 2003. Essential Mathematical Biology. Springer, London.

69. Shaw, J. E., J. R. Alattia, J. E. Verity, G. G. Prive, and C. M. Yip. 2006. Mechanisms of antimicrobial peptide action: studies of indolicidin assembly at model membrane interfaces by in situ atomic force microscopy. *J. Struct. Biol.* 154:42–58.

70. Brogden, K. A. 2005. Antimicrobial peptides: pore formers or metabolic inhibitors in bacteria? *Nat. Rev. Microbiol.* 3:238–250.

71. Toke, O. 2005. Antimicrobial peptides: new candidates in the fight against bacterial infections. *Biopolymers.* 80:717–735.